IJMMM International Journal of Minerals, Metallurgy and Materials 矿物冶金与材料学报（英文版）

Microstructure and phase elemental distribution in high-boron multi-component cast irons

Yu.G. Chabak, K. Shimizu, V.G. Efremenko, M.A. Golinskyi, K. Kusumoto, V.I. Zurnadzhy, and A.V. Efremenko

Cite this article as:
Yu.G. Chabak, K. Shimizu, V.G. Efremenko, M.A. Golinskyi, K. Kusumoto, V.I. Zurnadzhy, and A.V. Efremenko, Microstructure and phase elemental distribution in high-boron multi-component cast irons, *Int. J. Miner. Metall. Mater.*, 29(2022), No. 1, pp. 78-87. https://doi.org/10.1007/s12613-020-2135-8

View the article online at SpringerLink or IJMMM Webpage.

International Journal of Minerals, Metallurgy and Materials
Volume 29, Number 1, January 2022, Page 78
https://doi.org/10.1007/s12613-020-2135-8

Microstructure and phase elemental distribution in high-boron multi-component cast irons

Yu.G. Chabak[1)], *K. Shimizu*[2)], *V.G. Efremenko*[1),✉], *M.A. Golinskyi*[1)], *K. Kusumoto*[2)], *V.I. Zurnadzhy*[1)], *and A.V. Efremenko*[1)]

1) Physics Department, Pryazovskyi State Technical University, Mariupol, 87555, Ukraine
2) Mechanical Engineering Research Unit, College of Design and Manufacturing Technology, Muroran Institute of Technology, Muroran-city, 050-8585, Japan
(Received: 25 May 2020; revised: 5 July 2020; accepted: 7 July 2020)

Abstract: The novel cast irons of chemical composition (wt%) 0.7C–5W–5Mo–5V–10Cr–2.5Ti were invented with the additions of 1.6wt% B and 2.7wt% B. The aim of this work was to study the effect of boron on the structural state of the alloys and phase elemental distribution with respect to the formation of wear-resistant structural constituents. It was found that the alloy containing 1.6wt% B was composed of three eutectics: (a) "$M_2(C,B)_5$+ferrite" having a "Chinese Script" morphology (89.8vol%), (b) "$M_7(C,B)_3$+Austenite" having a "Rosette" morphology, and (c) "M_3C+Austenite" having a "Ledeburite"-shaped morphology (2.7vol%). With 2.7wt% of boron content, the bulk hardness increased from HRC 31 to HRC 38.5. The primary carboborides $M_2(C,B)_5$ with average microhardness of HV 2797 appeared in the structure with a volume fraction of 17.6vol%. The volume fraction of eutectics (a) and (b, c) decreased to 71.2vol% and 3.9vol%, respectively. The matrix was "ferrite/austenite" for 1.6wt% B and "ferrite/pearlite" for 2.7wt% B. Both cast irons contained compact precipitates of carbide (Ti,M)C and carboboride (Ti,M)(C,B) with a volume fraction of 7.3%–7.5%. Based on the energy-dispersive X-ray spectroscopy, the elemental phase distributions and the appropriate phase formulas are presented in this work.

Keywords: multi-component cast iron; boron; eutectic; carbide; carboboride

1. Introduction

Improving the operational durability of machine parts and tools is a challenging issue [1–4], which fundamentally depends on the correct selection of material. For many manufacturing processes, such as in mining, cement production, metallurgy, the use of wear-resistant alloys of various alloying systems, including white cast irons [5–7], is effective. The chemical composition and processing technology of these alloys are continuously improving by employing novel approaches. The group of wear-resistant cast irons includes multi-component cast irons developed in the mid-1990s [8–10]. These cast irons are alloys formed with several strong carbide-forming elements (Cr, V, W, and Mo) in approximately equal proportions, focusing on the formation of a multiphase structure consisting of hard carbides M_7C_3, M_6C, M_2C, and MC embedded into the austenite/martensite matrix [11–12]. The composite-shaped structure of multi-component cast irons is beneficial for its exploitation characteristics. Therefore, they are successfully utilized for the rolls of hot-strip mills and elements of pulverizing mills in cement industry [13]. Alternatively, the multi-component cast iron may contain other elements (Nb, Ni, and Co) to improve the properties, such as wear resistance, hardenability, and high-temperature erosion [14–16].

Another concept of developing wear-resistant high-boron cast irons is based on partial replacement of a carbon by boron [17–19]. These alloys contain up to 3.5wt% B (with optional alloying by chromium) that forms the boride or carboboride-based eutectic. The hardness of these borides is usually higher when compared with that of the carbides formed by the same elements [20–23]. This ensures improved wear behavior of the high-boron cast irons [24–26]. Jian *et al.* [25] found that the wear behavior of high-boron alloy can be increased by adding chromium, which improves the toughness of borides. Zhang *et al.* [26] reported the excellent wear resistance of Fe–Si–Mn–Cr with 2wt% B alloy attributed to the synergy between the high-hardness borides (M_3B_2 and M_2B) and the softer matrix composed of bainite and retained austenite. Cui *et al.* [27] studied about hot (800°C) wear resistance of Fe–Cr–B alloys containing up to 9wt% of boron and concluded that the specific wear rates of B-containing specimens were 1/10 of the unreinforced specimen. In present work, a novel approach is proposed, which is the combination of both the above concepts to develop a multi-component high-boron cast iron. In this study, we focused on the investigation of the microstructural features and elemental phase-distribution behavior of W–Mo–V–Cr–Ti

✉ Corresponding author: V.G. Efremenko E-mail: vgefremenko@gmail.com

cast irons with different boron contents.

2. Experimental

In a 25-kg induction furnace, the novel multi-component high-boron cast irons were smelted and poured into sand molds to obtain a Y-shaped casting. The target chemical composition (wt%) of the alloys was selected as 0.7C–1Si–1Mn–5W–5Mo–5V–10Cr–2.5Ti with different boron contents (1.5wt% and 2.5wt%). The cast irons were smelted using charge materials, such as steel scrap, pig iron, and the master-alloys of FeW, FeMo, FeCr, FeV, FeMn, FeSi, FeTi, and FeB. Boron was added to the molten mixture before it is pouring. The chemical compositions of the obtained alloys are presented in Table 1. The alloys were designated as 1.6B and 2.7B according to their actual boron content which slightly differed from the target one. The cast irons were poured into the sand molds. After knocking, the Y-shaped castings were cut to prepare the specimens for further investigation.

Table 1. Chemical composition of the alloys studied wt%

Alloy	C	B	Si	Mn	Cr	Mo	V	W	Ti	Al	Fe
1.6B	0.77	1.62	1.12	1.16	10.45	5.38	4.97	5.84	2.93	0.05	Bal.
2.7B	0.72	2.75	1.10	0.90	10.35	5.57	5.78	5.05	2.60	0.04	Bal.

The microstructure of the alloy was studied after etching with a 4vol% of nital solution (solution of nitric acid and alcohol) using a Nikon Eclipse M200 optical microscope (OM) and a JEOL JSM-6510 scanning electron microscope (SEM). The phase chemical composition and elemental distribution were determined by the EDX (energy-dispersive X-ray spectroscopy) method using a JEOL JED-2300 detector. The phase chemical composition of the alloys was studied by X-ray diffraction (XRD) using a Rigaku IV Pro diffractometer with Cu-K_α radiation. The hardness was measured by Rockwell method (scale C) and the microhardness was measured using Future-Tech FM-300 hardness tester with a load of 20 g. The prediction of phase constituents of the alloys was fulfilled by Thermo-Calc software.

Using optical micrographs of the structure, the volume fractions of the structural components were calculated by the Rosiwal lineal method [28]. To find the average of the results, ten micrographs of 440 μm × 600 μm area of the same magnification for each alloy were used.

3. Results

3.1. Thermodynamic modeling

For the evaluation structural formation of alloys, the thermodynamic calculations were performed using the Thermo-Calc software. The temperature sequence of phase appearances is presented in Table 2. In alloy 1.6B, solidification starts at 1451°C and titanium carbide (TiC) first solidifies from the melt. Then, tungsten boride WB appears at 1358°C. Ferrite with bcc (body-centered cubic) lattice starts forming from 1230°C as a result of sequential eutectic transformations with the formation of boride WB and boride MoB (begins from 1125°C). At 1030°C, another eutectic transformation starts leading to the formation of chromium carbide M_7C_3 crystallization. Titanium boride (TiB_2) appears at 950°C, whereas chromium borides (Cr_2B and Cr_4B) appear at much lower temperatures (633 and 550°C, correspondingly).

In alloy 2.7B, the set of equilibrium phases is same as for alloy 1.6B, but there are some differences. The solidification begins from the crystallization of tungsten boride WB that appears at a much higher temperature (1470°C) than that of alloy 1.6B. The crystallization of chromium carbide (M_7C_3) starts at 996°C, which is lower than that of alloy 1.6B. Similarly, iron boride (Fe_2B) appears at 938°C, which was not predicted in alloy 1.6B.

3.2. Microstructure and hardness

Fig. 1 shows the optical images of 1.6B alloy microstructure. It can be seen that these are neither matrix dendrites nor primary carbides or borides). So, the chemical composition of the alloy is near to a eutectic point (Fig. 1(a)). The structure is composed of three types of eutectics. The major (in area fraction) eutectic is seen as the vast colonies, which is consisting of dark contrast prolonged hard phase fibers (0.2–0.5 μm thickness) embedded in a light-contrast matrix (Fig. 1(b)). The fibers diverged from the colony center in a radial direction, at an angle of approximately 120°, making the periphery of the colony sparser, while the fibers simultaneously become thicker (up to 3 μm). Morphologically, this eutectic is similar to that of a "Chinese Script" eutectic, which is the characteristic of the light metal-based cast alloys [29–30]. The eutectic fibers starts crystallizing on the periphery in a Γ-shape or Π-shape contouring the colony borderline. The 90° angle of the colony borderline is shown in Fig. 1(b) by the double arrow. This kind of eutectic ("Chinese Script"-shaped) is denoted by E_1.

Two other types of eutectics with different morphologies are observed in the gaps between the vast "Chinese Script"

Table 2. Starting temperature (t_s) of equilibrium phase solidification °C

Alloy	TiC	WB	bcc	MoB	M_7C_3	TiB_2	Cr_2B	Cr_4B	Fe_2B
1.6B	1451	1358	1230	1125	1030	950	633	550	—
2.7B	1443	1470	1125	1125	996	970	555	—	938

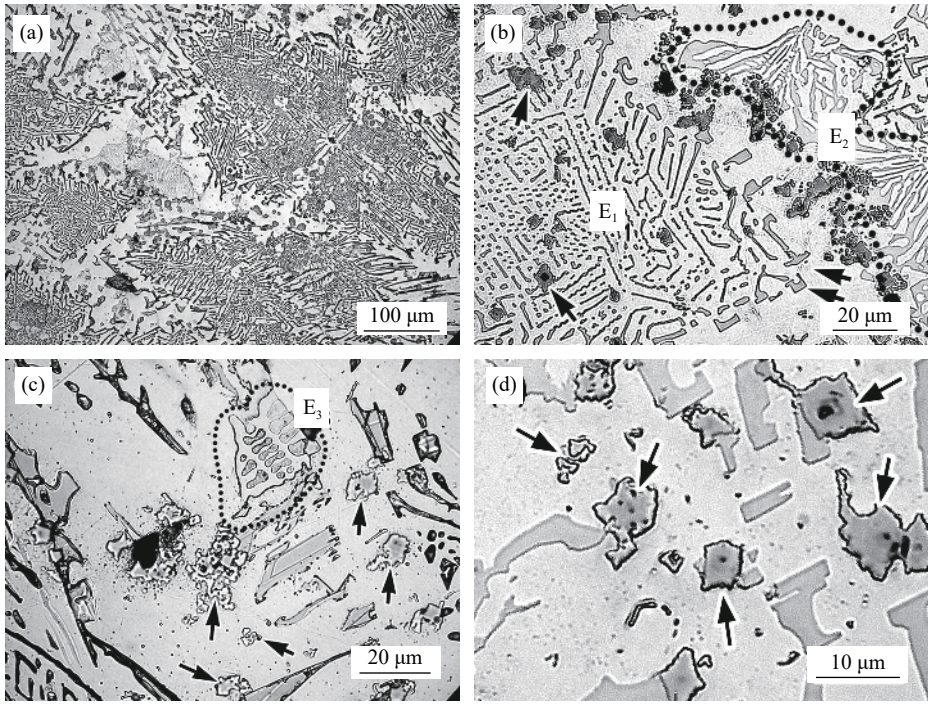

Fig. 1. Microstructure of the 1.6B alloy: (a) a total view; (b) "Chinese Script" eutectic and "Rosette" eutectic; (c) "Ledeburite"-shaped eutectic; (d) compact precipitates. The eutectics E_2 and E_3 are circled by the dotted line.

eutectic colonies. One of these eutectics has a "Rosette"-shaped morphology, which is specific for the M_7C_3 carbide-based eutectic in high-chromium cast irons [31]. The morphological feature of the "Rosette" eutectic is rod-shaped or plate-shaped hard phase precipitates branched inside the solid solution matrix (Fig. 1(b)). The hard inclusions are much thicker than that of the "Chinese Script" eutectics. The "Rosette" eutectic is denoted by E_2. Another type of eutectic has "honeycomb"-shaped morphology, which consists of portions of solid solution matrix embedded in the carbide matrix (circled by the dotted line in Fig. 1(c)). This type of eutectic is specific for the cementite-based eutectic ("Ledeburite"-shaped) in low-chromium white cast irons [32] and denoted by E_3. In addition to the structural components of the eutectics, equiaxed compact precipitates of the hard phase are revealed in the structure to be randomly distributed in the alloy (shown in Fig. 1(d) by the arrows). They have a close-to-rectangular shape structure with wavy contours. The precipitate size is 1.5–9 μm with average values of approximately 5 μm.

The volume fractions of "Chinese Script" eutectic and compact precipitates were measured as (89.8±17.2)vol% and (7.5±1.1)vol%, respectively. Since, accurate identification of the eutectics E_2 and E_3 in the structure was difficult, the total area fraction of the eutectics (E_2 + E_3) was counted to be (2.7±0.7)vol%.

Fig. 2 represents the microstructure of 2.7B alloy. Its distinct feature is the coarse centrally holed primary precipitates of rectangular shape with a side of up to 150 μm length (Fig. 2(a)). From these inclusions, the colonies of "Chinese Script" eutectic grow. The mix of different eutectics (E_1, E_2, and E_3) is seen (Fig. 2(b)) in between the gaps of the primary inclusions. Fig. 2(a) and (b) present the backscattered electron composition (BEC) images of the primary inclusions, the fibers of "Chinese Script" eutectic, and the equiaxed compact precipitates having a light contrast, which means that they are enriched with the elements of heavy metals (W, Mo) having higher atomic numbers [33]. However, eutectics E_2 and E_3 have a dark contrast, i.e., they are enriched with elements of lower atomic number (V, Cr, Mn, Fe). In comparison with the alloy 1.6B, the matrix of alloy 2.7B comprised the pearlite-shaped areas consisting of fine lamellar (0.2–0.6 μm width) or grainy (0.2–0.7 μm diameter) precipitates (Fig. 2(c)). The volume fractions of the structural components of alloy 2.7B were counted as (17.6±6.0)vol% (primary precipitates), (71.2±16.0)vol% (E_1), (3.9±1.4)vol% (E_2 + E_3), and (7.3±0.4)vol% (compact precipitates) (Fig. 3).

The X-ray diffraction study of the 1.6B alloy revealed the following phase constituents, specifically: αFe-phase, γFe-phase, M_2B_5, M_7C_3, Ti_2B, M_3C, and TiC (Fig. 3). According to the XRD peaks intensity, the α-phase was predominant for the structure of the 1.6B alloy. Other high-intensity peak at $2\theta = 35.4°$ is close to the peaks of the borides W_2B_5, Ti_2B_5, and Mo_2B_5. Therefore, the stoichiometry of this phase was suggested as M_2B_5 (where M = W, Mo, or Ti). The rest of the phases showed peaks of XRDs with low intensity, indicating a decreased volume fraction. In the 2.7B alloy, the same set of phase constituents were found, while the intensities of the peaks for the M_2B_5 phase at $2\theta = 35.4°$ was lower than that of the 1.6B alloy. Instead, the intensive peak at $2\theta = 43.5°$ appeared, which could be attributed to γFe-phase or to borides (W_2B_5 and Ti_2B_5). As no other peaks of austenite are observed on XRD pattern for the 2.7B alloy, the peak at $2\theta = 43.5°$ generally relates to boride M_2B_5 than to austenite. This enabled the conclusion that the higher XRD response in M_2B_5 peaks intensity was due to the appearance of coarse primary

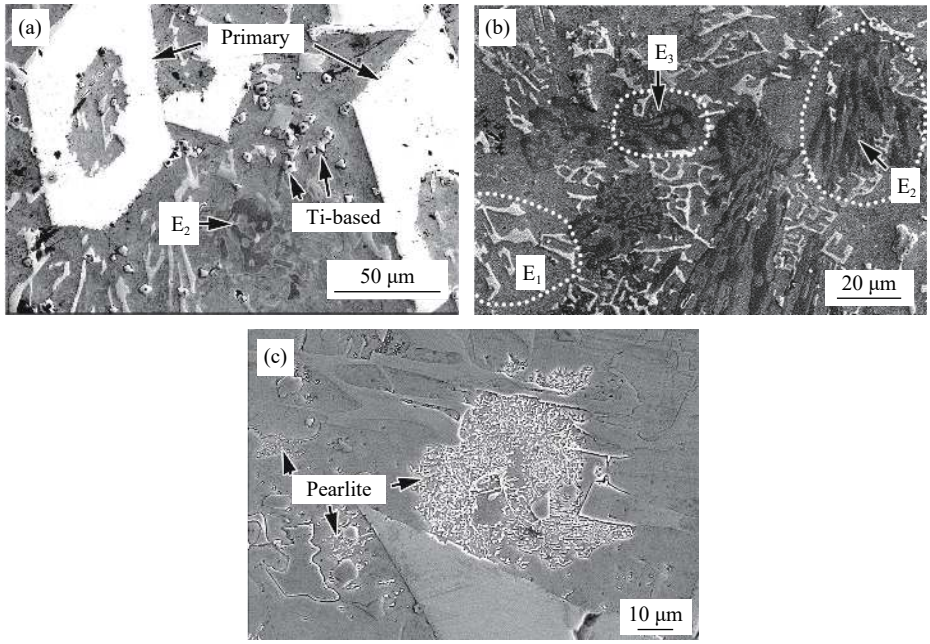

Fig. 2. Microstructure of the 2.7B alloy: (a) total view (BEC-image); (b) eutectic E_1 (light contrast) and eutectics E_2/E_3 (dark contrast) (BEC-image); (c) pearlite areas within the matrix (secondary electron image (SEI)).

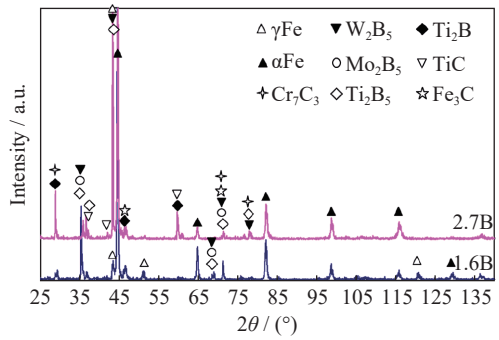

Fig. 3. XRD patterns for the 1.6B alloy and 2.7B alloy.

inclusions.

According to the measurements by XRD and microstructural observation, the matrix in the alloys was "ferrite/austenite" in the 1.6B alloy and "ferrite/pearlite" in the 2.7B alloy.

The average bulk hardness values of the alloys 1.6B and 2.7B were measured as HRC 31 and HRC 38.5, respectively. The microhardness of the structural components of 1.6B alloy was measured as HV 426±66 for "Chinese Script" eutectic and HV 836±153 for E_2/E_3 eutectics. The microhardness of the 2.7B alloy structural components was measured as HV 557±136 ("Chinese Script" eutectic), HV 745±91 (E_2/E_3 eutectics), HV 514±42 (ferrite/austenite matrix), HV 488±45 (pearlite matrix), and HV 2797±191 (bulk primary precipitates). The microhardness of the compact precipitates and eutectic hard fibers was not measured owing to their small sizes.

3.3. Phase elemental distribution

Figs. 4 and 5 present the EDX-mapping of the elemental distribution, where the element content refers to the color scale shown on the left side of the map. Fig. 4 shows the 1.6B alloy featuring the colonies of "Chinese Script" eutectic with occasional E_2/E_3 eutectic colonies lying in the gaps between the E_1 colonies. Eutectics E_2 and E_3 are not seen in the BEC-image (Fig. 4(a)) because of the dark contrast. Therefore, they are marked with a dotted line in the image.

As seen in Fig. 4(b–d), the fibers of the hard phase in the "Chinese Script" eutectic are significantly enriched by W, Mo, and V. The tungsten content in the "Chinese Script" eutectic exceeds that of the molybdenum and vanadium contents. The Cr content in E_1 is moderate. Iron is not evenly distributed in the E_1 fibers, the Fe content starts from zero in the coarse fibers to moderate in the fine fibers. Titanium is mostly concentrated on the compact inclusions to be slightly dissolved in the E_1 fibers. The sites of the E_2/E_3 eutectics are seen in Fig. 4(e) and (f) as the light-contrast areas to be enriched by chromium and iron. The content of Fe in the E_2/E_3 eutectic matrices is higher than the contents of Mo and V. W and Ti are absent in E_2/E_3. The matrix of the 1.6B alloy is enriched by Fe and Cr and depleted of other alloying elements (Fig. 4(f)).

In 2.7B alloy, the primary bulk precipitates have a high content of W, Mo, and V (Fig. 5(b–d)) and they also contain a certain amount of Cr and Ti (Fig. 5(e) and (f)). However, these precipitates are almost completely depleted of iron (Fig. 5(g)). The same elemental distribution is the characteristic for "Chinese Script" eutectic, which proves that the hard phase in E_1 is heavily alloyed by W, Mo, and V. In contrast, the E_2/E_3 eutectics have high contents of Cr and Fe. Titanium is generally concentrated on the compact equiaxed precipitates.

The mapping of EDX was supplemented by EDX point analysis performed at different phase constituents, such as the fibers of "Chinese Script" eutectic, the fibers of "Rosette" eutectic (E_2), the compact precipitates, and the matrix. Fig. 6 shows the EDX spectra, which clearly depicts the difference in phase elemental composition. Figs. 7 and 8 represent the average phase chemical compositions of the 1.6B and 2.7B

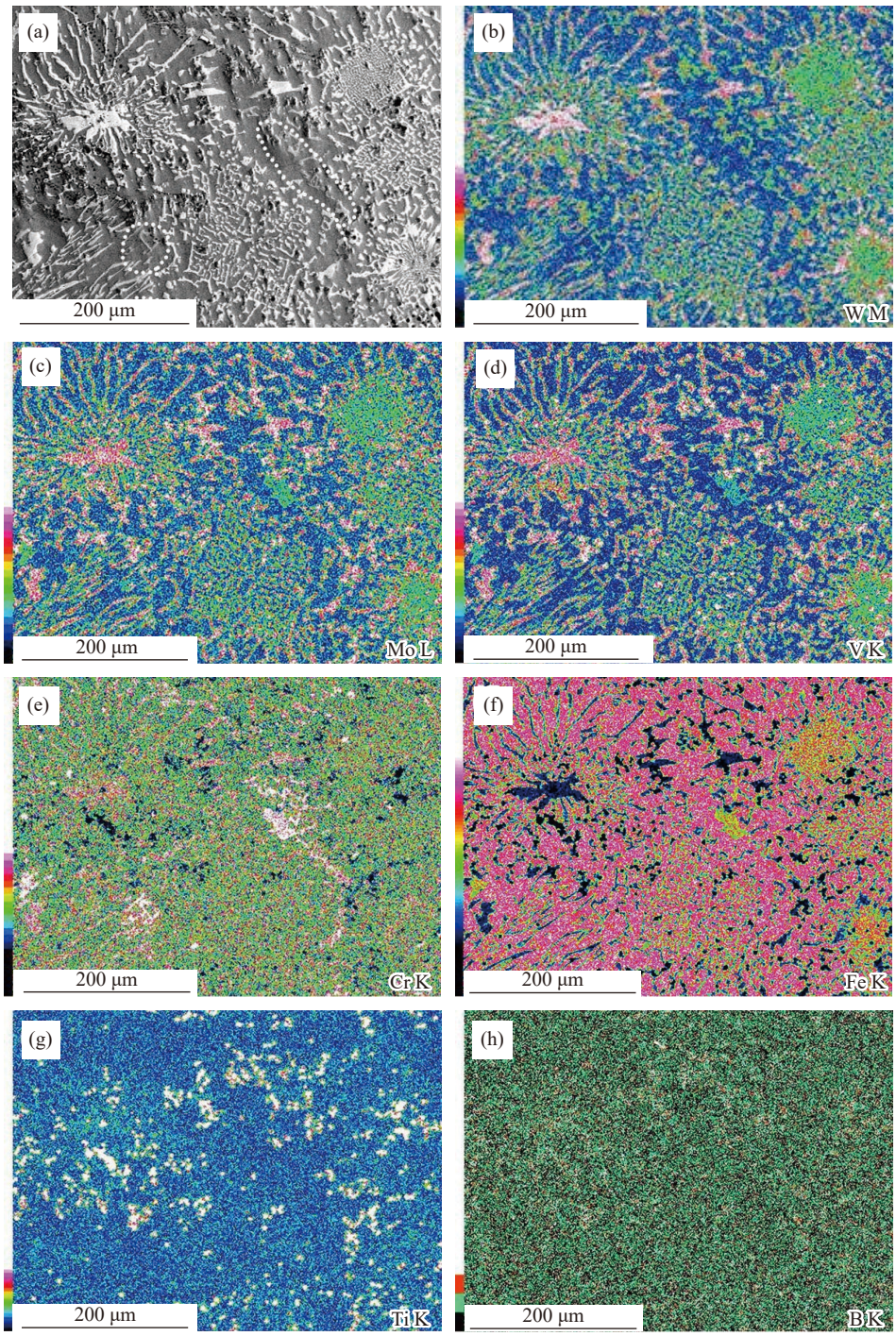

Fig. 4. Phase elemental distribution in 1.6B alloy: (a) SEI-image; (b) W; (c) Mo; (d) V; (e) Cr; (f) Fe; (g) Ti; (h) B. Eutectic E_2 area is shown in (a) by the dotted line.

alloys, respectively. In the 1.6B alloy, the fibers of "Chinese Script" eutectic specially consisted of 11.1±1.5 B, 3.9±0.8 C, 0.3±0.04 Ti, 17.5±1.4 V, 15.8±2.0 Cr, 14.0±0.4 Mo, 16.4±1.9 W, 0.2±0.1 Mn, and 20.8±1 Fe in wt%. This composition verifies that the fibers of "Chinese Script" eutectic are carboborides. The fibers of "Rosette" eutectic appeared as the carbides: 6.9±0.1 C, 0.3±0.03 Ti, 11.8±1.3 V, 38.9±6.8 Cr, 3.8±0.8 Mo, 2.0±0.7 W, 1.2±0.5 Mn, and 35.1±7.1 Fe in wt%. The chemical compositions of the compact precipitates are allowed identifying them as carboborides: 4.83±1.5 B, 12.5±1.6 C, 49.9±8.3 Ti, 12.9±1.5 V, 1.1±0.3 Cr, 0.2±0.1 Mn, 3.48±1.2 Fe, and 15.1±1.6 W in wt%. The matrix of the 1.6B alloy consisted of: 2.6±0.07 C, 9.9±1.6 Cr, 1.2±0.2 Mo, 1.3±0.2 V, 0.6±0.2 W, and 85.3±0.3 Fe in wt%.

In the 2.7B alloy, the primary coarse precipitates contained W ((22.0±1.7)wt%), V ((16.1±0.5)wt%), and Mo ((15.3±0.3)wt%) with a lower amount of Cr ((11.3±0.6)wt%) and Ti ((2.5±0.2)wt%). Iron was also present in the coarse inclusions in the amount of (18.1±0.3)wt%. The distinct feature of these precipitates was the presence of C ((5.1±0.3)wt%) and B ((9.3±1.0)wt%), indicating that they were carboborides. "Chinese Script" fibers had approxim-

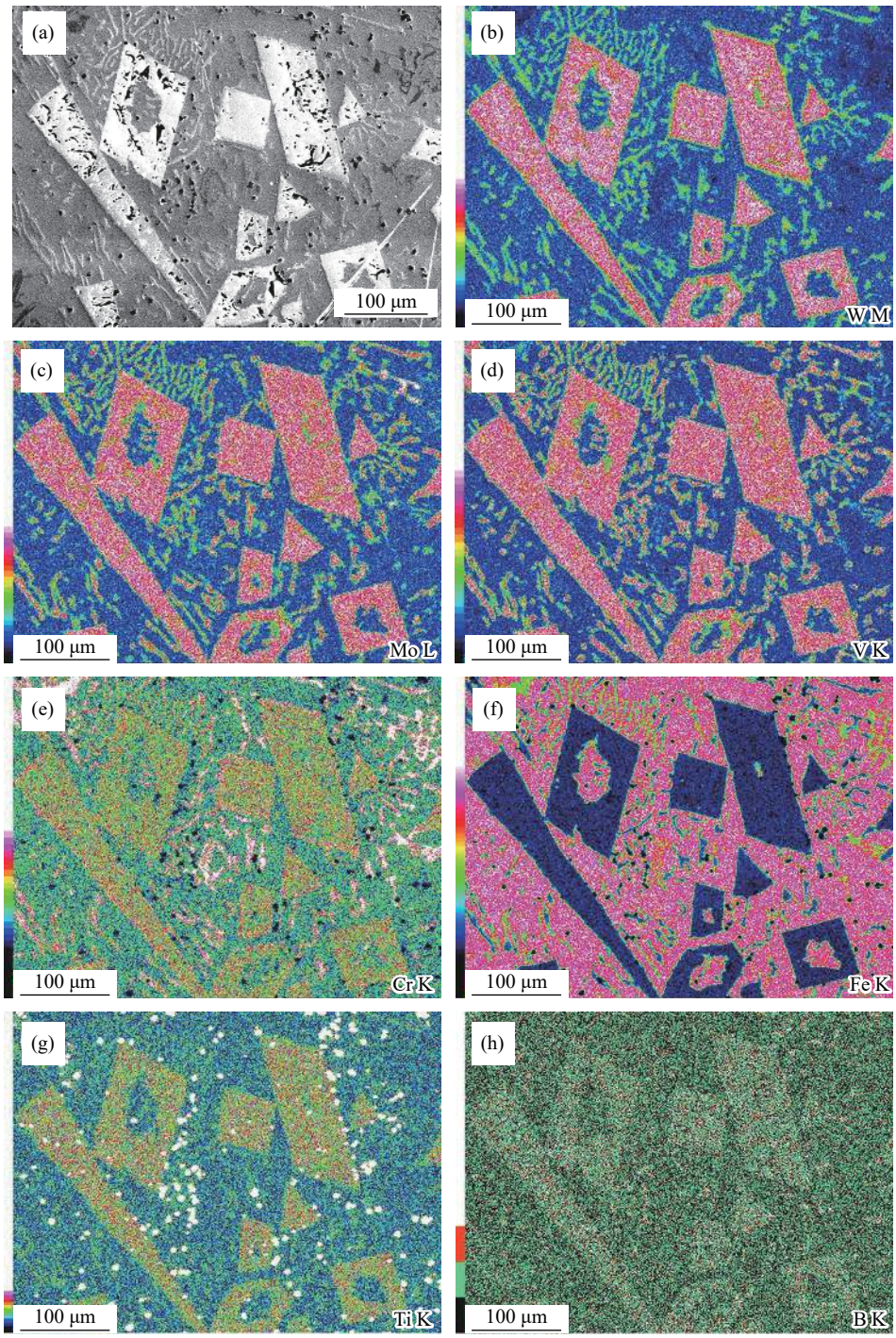

Fig. 5. Phase elemental distribution in 2.7B alloy:(a) SEI-image; (b) W; (c) Mo; (d) V; (e) Cr; (f) Fe; (g) Ti; (h) B.

ately the same chemical compositions as that of the 1.6B alloy (11wt%–18wt% of W, Mo, V, and Cr each, and 1.5±0.2 Ti, 23.4±0.3 Fe, 10.4±0.7 B, and 4.6±0.5 C in weight percent).

The fibers of the E_2 eutectics had heterogeneity for boron and carbon, which varied in the range of 0–6.0wt% and 2.9wt%–4.9wt%, respectively. As compared with the 1.6B alloy, the content of Cr in E_2fibers was lowered by almost 10wt% ((27.5±0.5)wt%). The chemical composition of the compact Ti-based precipitates was: 8.8wt% C, 69.6wt% Ti, 7.6wt% V, 3.4wt% Mo, and 10.6wt% W. The matrix of the alloy 2.7B contained (8.3±0.3)wt% Cr and (1.3±0.2)wt% V.

4. Discussion

As mentioned above, the cast irons being studied had a multi-phase status. The cast irons were alloyed by several carbide(boride)-forming elements which can be divided into four groups according to their carbide (or boride) affinity: (a) Fe and Mn (weak), (b) Cr (moderate), (c) W, Mo, and V (strong), and (d) Ti (very strong) [34]. All these elements compete with each other to bound with carbon and boron under the alloy solidification. Eventually, four main hard phase constituents appeared: (a) Ti-based, (b) W-, Mo-, and V-based, (c) Cr-based, and (d) Fe-based as measured by XRD.

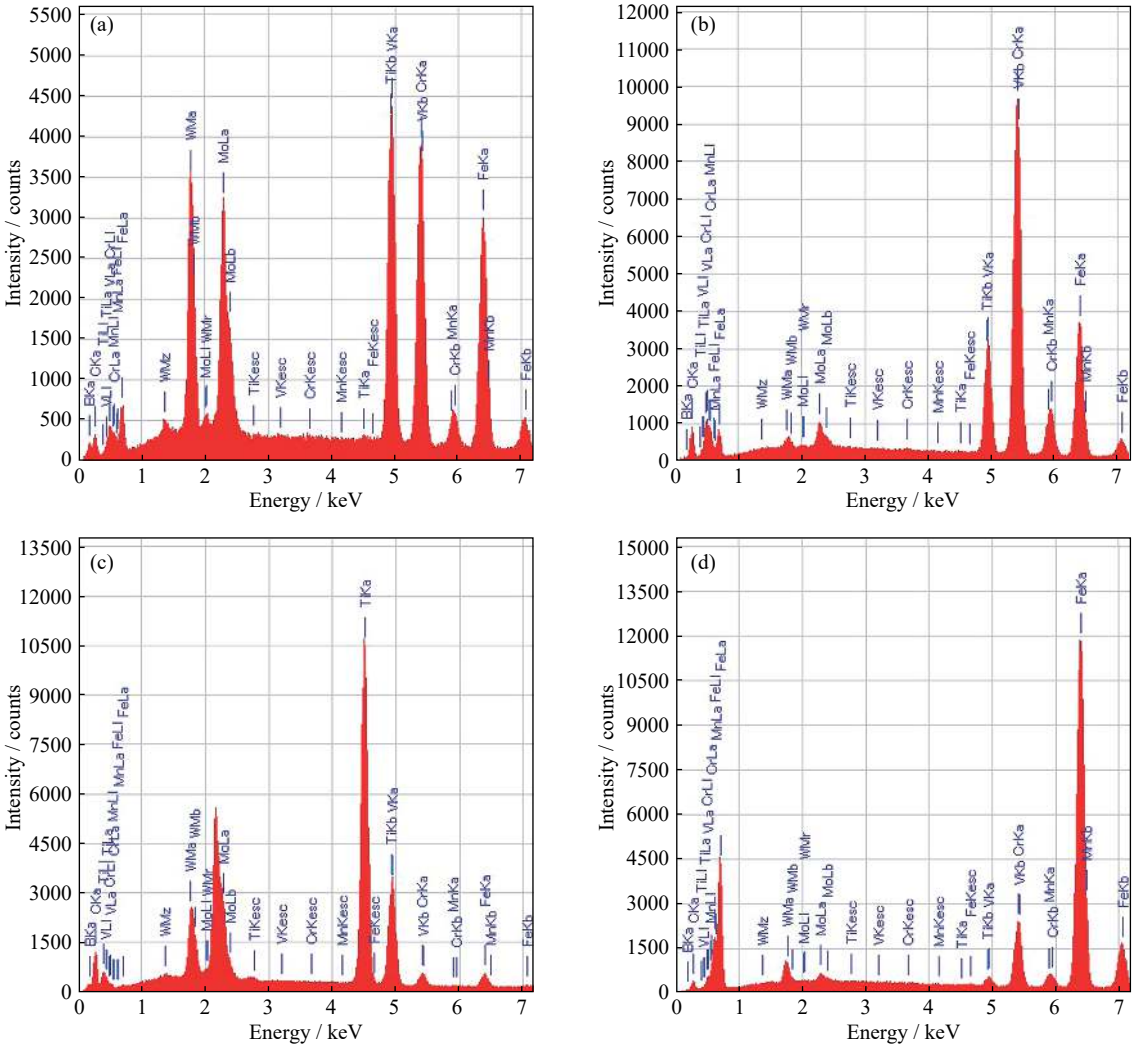

Fig. 6. EDX spectra of the 1.6B alloy: (a) fiber of "Chinese Script" eutectic; (b) fiber of "Rosette" eutectic (E_2); (c) compact precipitate; (d) matrix.

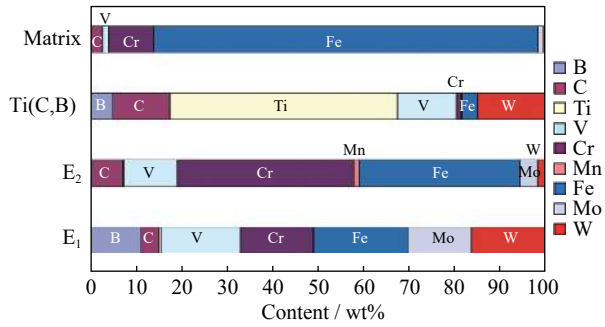

Fig. 7. Phase chemical composition of 1.6B alloy (fibers of E_1 eutectic, fibers of E_2 eutectic, TiB_2 precipitate, TiC precipitate, and matrix).

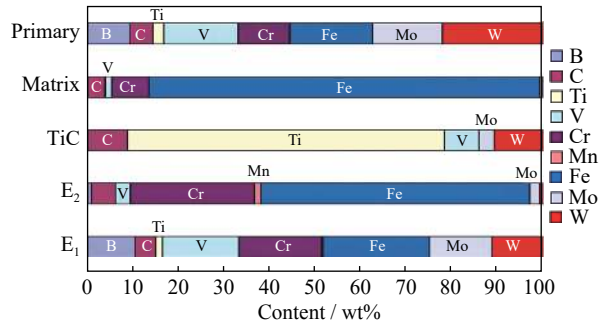

Fig. 8. Phase chemical compositions of 2.7B alloy (fibers of E_1 eutectic, fibers of E_2 eutectic, TiC precipitate, primary precipitate, and matrix).

Alloying with titanium caused the formation of Ti-rich precipitates of compact shape. The XRD study showed the presence of Ti_2B and TiC compounds. The EDX examination allowed to reveal carboboride (Ti,M)(C,B) in the 1.6B alloy and carbide (Ti,M)C in the 2.7B alloy (where M = W, V, Mo, or Fe). According to EDX data, the chemical composition of titanium carboboride was represented by the stoichiometric formula $(Ti_{0.39}W_{0.46}V_{0.11}Fe_{0.03})(C_{0.7}B_{0.3})$, whereas the formula to represent titanium carbide was calculated as $(Ti_{0.6}W_{0.30.1}Mo_{0.1})C$. The precipitates with appropriate TiB_2 elemental composition were not found during the EDX study.

The phases (Ti,M)C and (Ti,M)(C,B) have the same morphological features making them difficult to be visually distinguished in the structure. For the first site, these phases are seemed evenly distributed in the structure. However, the analysis of the mapping images (Figs. 3(g) and 4(g)) reveals that Ti-rich precipitates are generally concentrated on the periphery of the E_1 eutectic colonies (1.6B alloy) or on the peri-

meter of the primary carboborides (2.7B alloy). This type of distribution suggests that the Ti-rich precipitates solidified before the primary carboboride formation (or before the eutectic reactions) to be further pushed aside to the liquid by growing carboborides or eutectic colonies. Some Ti-rich precipitates are located inside the coarse inclusions, representing that precipitates of (Ti,M)C and (Ti,M)(C,B) acted as the nuclei for primary carboborides.

The trio of strong carbide- and boride-forming elements "W–Mo–V" with a total amount of 15wt%, bind most of the boron and carbon atoms to form carboboride, $M_2(B,C)_5$. In the 1.6B alloy, the carboboride $M_2(B,C)_5$ crystallizes through the eutectic reaction "L→αFe + $M_2(B,C)_5$" as a fiber of "Chinese Script" eutectic. According to the EDX data, the stoichiometry of $M_2(B,C)_5$ fibers in the 1.6B alloy is presented as $(W_{0.8}Mo_{0.4}Fe_{0.3}V_{0.2}Cr_{0.2})(C_{1.4}B_{3.6})$. Thus, chromium and iron are partially dissolved in this carboboride. The matrix is depleted of W, Mo, and V as the contents of Mo and V in the matrix are less than 2wt% and the content of W is negligible in the matrix.

Chromium is more uniformly partitioned between the phases than that of the stronger carbide-forming elements with its concentration in the matrix reaching approximately 9wt%. Since, chromium was added in a much higher content (10wt%), it was able to bind a certain part of carbon to form a minor amount of "Rosette" eutectic (austenite + M_7C_3). The "Rosette" eutectics appear in the areas depleted of W, Mo, and V. As "Rosette" eutectic carbide M_7C_3 is contained W, Mo, V, and Fe, its formula for the 1.6B alloy is $(Cr_{2.6}Fe_{2.6}V_{0.8}W_{0.5}Mo_{0.5}Mn_{0.1})C_3$. In the areas depleted of chromium, the "Ledeburite"-shaped eutectic (E_3) solidified.

As W, Mo, and V are strong ferrite stabilizers and ferrite and austenite are present in the 1.6B alloy, it can be assumed that the ferrite belongs to the "Chinese Script" eutectic matrix, whereas austenite was the matrix of the "Rosette" eutectic and "Ledeburite"-shaped eutectic. This assumption corresponds to the "ferrite/austenite" volume fraction ratio (XRD data) "$E_1/(E_2+E_3)$" volume fraction ratio (according to the OM observation).

The increasing amount of boron content to 2.7wt% altered the status of alloy from "eutectic" to "hypereutectic". This revealed the crystallization of coarse primary rectangular-shaped carboborides $M_2(B,C)_5$ of stoichiometry $(W_{1.0}Mo_{0.36}Fe_{0.25}V_{0.21}Cr_{0.15}Ti_{0.03})(C_{1.9}B_{3.1})$. The microhardness of these precipitates (approximately HV 2600–3000) is higher than that of the tungsten carbides W_2C (HV 1700 [32]) and WC (HV 2200–2400 [35–36]). The hardness increased by adding more boron and by complex alloying. One can assume that the similar microhardness is also the characteristics of the carboborides in the "Chinese Script" eutectic. The volume fraction of primary carboboride was 17.6vol%; hence, they accumulated a significant part of W, Mo, V, and Cr from the liquid phase before the eutectic reactions during crystallization process. As a result, the $M_2(B,C)_5$ fibers of "Chinese Script" eutectic were depleted by tungsten in favor of chromium and iron and it can be represented by the formula $(W_{0.6}Mo_{0.4}Fe_{0.4}V_{0.2}Cr_{0.3})(C_{1.7}B_{3.4})$. Similarly, the fibers of "Rosette"-shaped eutectic were depleted of Cr, Mo, W, and V in favor of iron and boron. Thus, carbide M_7C_3 changed to carboboride $M_7(C,B)_3$ which can be represented by the formula $(Fe_{4.3}Cr_{1.8}Mo_{0.3}V_{0.2}W_{0.1}Mn_{0.1})(C_{2.6}B_{0.4})$. The matrix of the 2.7B alloy was also depleted by W, Mo, V, and Cr, which caused a transformation of depleted austenite into pearlite during cooling to room temperature [37].

Generally, the revealed phase composition of the alloys corresponds to a thermodynamic calculation. The main difference between experimental and calculated results is, instead of separate sequential crystallization of borides of tungsten, molybdenum, vanadium, and chromium that under real conditions, a complex carboboride $M_2(B,C)_5$ was formed, including all of the above elements. Also, the presence of austenite in 1.6B alloy was not predicted by calculation. The appearance of austenite is caused by inhomogeneity in carbon distribution, which is a result of elemental liquation.

The increase in boron content affected the microhardness of the eutectic colonies of "Chinese script" and E_2/E_3, resulting in a difference between the alloys. This difference can be explained concerning the chemical composition and the size of the hard fibers (carbides or carboborides) included in the eutectic colonies. The microhardness of the eutectic is a complex (integral) value depending on the hardness and relative position/dimensions of the matrix and hard phase. In 2.7B alloy, "Chinese script" is harder because of the presence of thicker fibers, which is 0.5–1.8 μm for 2.7B alloy, whereas it is 0.2–0.5 μm for 1.6B alloy. Thus, thicker fibers increase the contribution of carboborides into the integral microhardness of "Chinese script" in 2.7B alloy in comparison with 1.6B alloy. On the contrary, 2.7B alloy shows lower microhardness of E_2/E_3 eutectic colonies. This can be attributed to the much lower (by 10wt%) content of the main element, chromium, in eutectic carbide M_7C_3 under the increase of boron as mentioned above.

This work shows that the experimental multi-component high-boron cast irons are composite-shaped materials containing an increasing number of very hard carboborides and carbides in the structure, which could be beneficial for the wear performances of the alloys.

5. Conclusions

This paper investigated the structural features of the multi-component cast iron alloys formed by 1.6wt%–2.7wt% of boron. We conclude the following observations based on the analysis of the results.

(1) Multi-component high-boron cast irons containing nominal (wt%) 0.7C–1Si–1Mn–5W–5Mo–5V–10Cr–2.5Ti were fabricated with different boron contents of 1.6wt% and 2.7wt%. It was found that the chemical composition of 1.6wt% B cast iron corresponds to a eutectic point. Its microstructure is consisted of fine eutectic carboborides and carbides embedded in a "ferrite/austenite" matrix. Specifically, the structural components of 1.6wt% B cast iron were

(a) "Chinese Script" eutectic "αFe+$(W,Mo,V,Cr,Ti)_2(B,C)_5$" (major in volume fraction), (b) the "Rosette"-shaped eutectic "γFe+$(W,Mo,V,Cr,Ti)_7C_3$", (c) "Ledeburite"-shaped eutectic "γFe+M_3C", and (d) Ti-rich precipitates.

(2) The increase in boron content to 2.7wt% resulted in "shifting" of the alloy to the hypereutectic domain that led to the appearance of coarse primary carboborides $(W,Mo,V,Cr,Ti)_2(B,C)_5$ of rectangular shape with a microhardness of HV 2797±191. This triggered a sharp depletion of eutectic carboborides and carbides by W, Mo, V, and Cr. The matrix was also depleted by Cr, Mo, and W, which resulted in the transformation of austenite into pearlite.

(3) Titanium carbides (Ti,W,Mo,V)C and carboborides (Ti,W,Fe,Cr,V)(C,B) of compact equiaxed shape were EDX-revealed in both cast irons to be preferentially distributed at the periphery of the eutectic colonies or primary carboborides, which demonstrates their crystallization before process of solidification of the primary carboborides and the eutectic reactions.

Acknowledgements

This work was financially supported by Ministry of Education and Science of Ukraine under the project No 0119U100080. The authors appreciate the help of Professor Hossam Halfa (Central Metallurgical Research and Development Institute, Cairo, Egypt) with thermodynamic calculations using Thermo-Calc software.

Conflict of Interest

The authors declare that they have no conflict of interest.

References

[1] O.P. Ostash, V.V. Kulyk, V.D. Poznyakov, O.A. Haivorons' kyi, L.I. Markashova, V.V. Vira, Z.A. Duriagina, and T.L. Tepla, Fatigue crack growth resistance of welded joints simulating the weld-repaired railway wheels metal, *Arch. Mater. Sci. Eng.*, 2(2017), No. 86, p. 49.

[2] A.M. Dubey, A. Kumar, and A.K. Yadav, Wear behaviour of friction stir weld joint of cast Al (4%–10%) Cu alloy welded at different operating parameters, *J. Mater. Process. Technol.*, 240(2017), p. 87.

[3] A. Anishchenko, V. Kukhar, V. Artiukh, and O. Arkhipova, Application of G. Lame's and J. Gielis' formulas for description of shells superplastic forming, *MATEC Web Conf.*, 239(2018), art. No. 06007.

[4] V.G. Efremenko, V.I. Zurnadzhi, Y.G. Chabak, O.V. Tsvetkova, and A.V. Dzherenova, Application of the Q-n-P-treatment for increasing the wear resistance of low-alloy steel with 0.75% C, *Mater. Sci.*, 53(2017), No. 1, p. 67.

[5] A. Gonzalez-Pociño, F. Alvarez-Antolin, and J. Asensio-Lozano, Erosive wear resistance regarding different destabilization heat treatments of austenite in high chromium white cast iron, alloyed with Mo, *Metals*, 9(2019), No. 5, art. No. 522.

[6] V.G. Efremenko, Y.G. Chabak, K. Shimizu, A.G. Lekatou, V.I. Zurnadzhy, A.E. Karantzalis, H. Halfa, V.A. Mazur, and B.V. Efremenko, Structure refinement of high-Cr cast iron by plasma surface melting and post-heat treatment, *Mater. Des.*, 126(2017), p. 278.

[7] A. Bedolla-Jacuinde, F. Guerra, I. Mejia, and U. Vera, Niobium additions to a 15%Cr–3%C white iron and its effects on the microstructure and on abrasive wear behavior, *Metals*, 9(2019), No. 12, art. No. 1321.

[8] Y. Matsubara, N. Sasaguri, K. Shimizu, and S. K. Yu, Solidification and abrasion wear of white cast irons alloyed with 20% carbide forming elements, *Wear*, 250(2001), No. 1-12, p. 502.

[9] M. Hashimoto, O. Kubo, and Y. Matsubara, Analysis of carbides in multi-component white cast iron for hot rolling mill rolls, *ISIJ Int.*, 44(2004), No. 2, p. 372.

[10] Y. Yokomizo, N. Sasaguri, K. Nanjo, and Y. Matsubara, Continuous cooling transformation behavior of multi-component white cast iron, *J. Jpn. Foundry Eng. Soc.*, 74(2002), No. 1, p. 9.

[11] J. Opapaiboon, M.S.N. Ayudhaya, P. Sricharoenchai, S. Inthidech, and Y. Matsubara, Effect of chromium content on heat treatment behavior of multi-alloyed white cast iron for abrasive wear resistance, *Mater. Trans.*, 60(2019), No. 2, p. 346.

[12] T. Meebupha, S. Inthidec, P. Sricharoenchai, and Y. Matsubara, Effect of molybdenum content on heat treatment behavior of multi-alloyed white cast iron, *Mater. Trans.*, 58(2017), No. 4, p. 655.

[13] S. Inthidech and Y. Matsubara, Effects of carbon balance and heat treatment on hardness and volume fraction of retained austenite of semi-multi-alloyed white cast iron, *Int. J. Metalcast.*, 14(2020), No. 1, p. 132.

[14] Y. Zhang, K. Shimizu, K. Kusumoto, H. Hara, and C. Higuchi, Influence of Ni addition on erosive wear characteristics of multi-component white cast iron at elevated temperature, *Wear*, 376-377(2017), p. 452.

[15] V.G. Efremenko, K. Shimizu, A.P. Cheiliakh, T.V. Kozarevs' ka, Y.G. Chabak, H. Hara, and K. Kusumoto, Abrasive wear resistance of spheroidal vanadium carbide cast irons, *J. Frict. Wear*, 34(2013), No. 6, p. 466.

[16] Y. Zhang, K. Shimizu, X.B. Yaer, K. Kusumoto, and V.G. Efremenko, Erosive wear performance of heat treated multi-component cast iron containing Cr, V, Mn and Ni eroded by alumina spheres at elevated temperatures, *Wear*, 390-391(2017), p. 135.

[17] S. Ma and J. Zhang, Wear resistant high boron cast alloy—A review, *Rev. Adv. Mater. Sci.*, 44(2016), p. 54.

[18] P. Christodoulou and N. Calos, A step towards designing Fe–Cr–B–C cast alloys, *Mater. Sci. Eng. A*, 301(2001), No. 2, p. 103.

[19] Y.X. Li, Z.L. Liu, and X. Chen, Development of boron white cast iron, *Int. J. Cast Met. Res.*, 21(2008), No. 1-4, p. 67.

[20] H.K. Zeytin, H. Yildirim, B. Berme, S. Duduoğlu, G. Kazdal, and A. Deniz, Effect of boron and heat treatment on mechanical properties of white cast iron for mining application, *J. Iron Steel Res. Int.*, 18(2011), No. 11, p. 31.

[21] I. Spiridonova, O. Sukhova, and O. Vashchenko, Multicomponent diffusion processes in boride-containing composite materials, *Metall. Nov. Tekhnol.*, 21(1999), No.2, p. 122.

[22] J.J. Zhang, J.C. Liu, H.M. Liao, M. Zeng, and S.D. Ma, A review on relationship between morphology of boride of Fe–B alloys and the wear/corrosion resistant properties and mechanisms, *J. Mater. Res. Technol.*, 8(2019), No. 6, p. 6308.

[23] Y.Z. Sun, J.B. Li, D. Wellburn, and C.S. Liu, Fabrication of wear-resistant layers with lamellar eutectic structure by laser surface alloying using the *in situ* reaction between Cr and B_4C, *Int. J. Miner. Metall. Mater.*, 23(2016), No. 11, p. 1294.

[24] Z.G. Chen, S. Miao, L.N. Kong, X. Wei, F.H. Zhang, and H.B. Yu, Effect of Mo concentration on the microstructure evolution and properties of high boron cast steel, *Materials*, 13(2020), No. 4, art. No. 975.

[25] Y.X. Jian, Z.F. Huang, J.D. Xing, X.T. Liu, L. Sun, B.C.

Zheng, and Y. Wang, Investigation on two-body abrasive wear behavior and mechanism of Fe–3.0wt%B cast alloy with different chromium content, *Wear*, 362-363(2016), p. 68.

[26] C.L. Zhang, S.H. Li, Y.H. Lin, J. Ju, and H.G. Fu, Effect of boron on microstructure evolution and properties of wear-resistant cast Fe–Si–Mn–Cr–B alloy, *J. Mater. Res. Technol.*, 9(2020), No. 3, p. 5564.

[27] G.J. Cui, Z.W. Yang, W.J. Wang, and G.J. Gao, Tribological properties of Fe(Cr)–B alloys at high temperature, *J. Cent. South Univ.*, 26(2019), No. 10, p. 2643.

[28] V.G. Efremenko, Y.G. Chabak, A. Lekatou, A.E. Karantzalis, and A.V. Efremenko, High-temperature oxidation and decarburization of 14.55 wtpct Cr-cast iron in dry air atmosphere, *Metall. Mater. Trans. A*, 47(2016), No. 4, p. 1529.

[29] B.J. Kim, S.S. Jung, J.H. Hwang, Y.H. Park, and Y.C. Lee, Effect of eutectic Mg_2Si phase modification on the mechanical properties of Al–8Zn–6Si–4Mg–2Cu cast alloy, *Metals*, 9(2019), No. 1, art. No. 32.

[30] E. Georgatis, A. Lekatou, A.E. Karantzalis, H. Petropoulos, S. Katsamakis, and A. Poulia, Development of a cast Al–Mg_2Si–Si *in situ* composite: Microstructure, heat treatment, and mechanical properties, *J. Mater. Eng. Perform.*, 22(2013), No. 3, p. 729.

[31] V. Efremenko, K. Shimizu, T. Pastukhova, Y. Chabak, M. Brykov, K. Kusumoto, and A. Efremenko, Three-body abrasive wear behaviour of metastable spheroidal carbide cast irons with different chromium contents, *Int. J. Mater. Res.*, 109(2018), No. 2, p. 147.

[32] M. Trepczyńska-Łent and E. Olejnik, Solidification front of oriented ledeburite, *Arch. Foundry Eng.*, 16(2016), No. 1, p. 124.

[33] T. Kowoll, E. Müller, S. Fritsch-Decker, S. Hettler, H. Störmer, C. Weiss, and D. Gerthsen, Contrast of backscattered electron SEM images of nanoparticles on substrates with complex structure, *Scanning*, 2017(2017), art. No. 4907457.

[34] M. Aksoy, O. Yilmaz, and M.H. Korkut, The effect of strong carbide-forming elements on the adhesive wear resistance of ferritic stainless steel, *Wear*, 249(2001), No. 8, p. 639.

[35] A. Nino, K. Takahashi, S. Sugiyama, and H. Taimatsu, Effects of carbon addition on microstructures and mechanical properties of binderless tungsten carbide, *Mater. Trans.*, 53(2012), No. 8, p. 1475.

[36] H.O. Pierson, *Handbook of Refractory Carbides &Nitrides: Properties, Characteristics,Processing and Applications*, Noyes Publications, Westwood, 1996.

[37] V.I. Zurnadzhy, V.G. Efremenko, K.M. Wu, A.Y. Azarkhov, Y.G. Chabak, V.L. Greshta, O.B. Isayev, and M.V. Pomazkov, Effects of stress relief tempering on microstructure and tensile/impact behavior of quenched and partitioned commercial spring steel, *Mater. Sci. Eng. A*, 745(2019), p. 307.